DEINTERCALATION OF AN ALKALI METAL FROM A 2D KAGOMÉ METAL

by
Johndavid Sabedra

A thesis submitted to Johns Hopkins University in conformity with the requirements for the degree of Master of Science

Baltimore, Maryland
August 2021

Abstract

Kagomé metals are a recently discovered class of quantum material that have the potential to underlie more efficient and novel computing devices, if appropriately tunable and harnessable. A prototypical kagomé metal, the structure of KV_3Sb_5 was previously discovered to be in the P6/mmm space group and to display a kagomé net of vanadium atoms with potassium ions intercalated between slabs of V-Sb. KV_3Sb_5 shows potential for accessible Fermi Energy (E_F) tuning due to possible ease of deintercalation of potassium from the compound. Previous work has demonstrated uncontrolled deintercalation by etching in hot HNO_3 as well as treatment with water. In this work, controlled deintercalation of potassium via $[I_2 + I^-]$ in acetonitrile (ACN) was explored. Using the change in lattice parameter ratios (c/a) as a proxy, the effect of initial electrochemical potential of the ACN solution on potassium occupancy is demonstrated. The occupancy was shown to depend on the initial electrochemical potential of the solution, but with other contributing factors. Further, it was observed that the electrochemical potential of the solution did have an effect on structural decomposition of KV_3Sb_5. The extent of decomposition was explored and was found have a linear dependence on initial electrochemical potential of the ACN solution used for deintercalation. AC susceptibility measurements of samples post-deintercalation show a change in behavior at ≈ 2K with a decrease in potassium occupancy and degree of decomposition. These results demonstrate the difficulty of precisely controlling alkali metal content while avoiding secondary products during the synthesis of kinetically stable phases, and provide guidance of the challenges that must be overcome to make controllable chemical tuning of kagomé metals, a prerequisite for their use in functional devices, a reality.

Advisor: Dr. Tyrel M. McQueen

Table of Contents

List of Tables

List of Figures

Introduction

Due to their potential for exhibiting emergent magnetic and electronic phenomena, materials possessing kagomé lattices have been the subject of much study. The structure of kagomé lattices (Figure 1) is the root of many of their rarer properties. In particular, kagomé materials have been studied as quantum spin liquid candidates, and as hosts for Dirac fermions that may provide more energy efficient modes of computing. The pattern of repeating triangular components of the lattice can lead to magnetic frustration, prohibiting magnetic order all the way down to T = 0 K, and displaying long range entanglement.[1,2] Because of these properties, quantum spin liquids have been of such great interest for potential realization of achievements in quantum computing advancements as well as the possible achievement of room temperature superconductivity.[3]

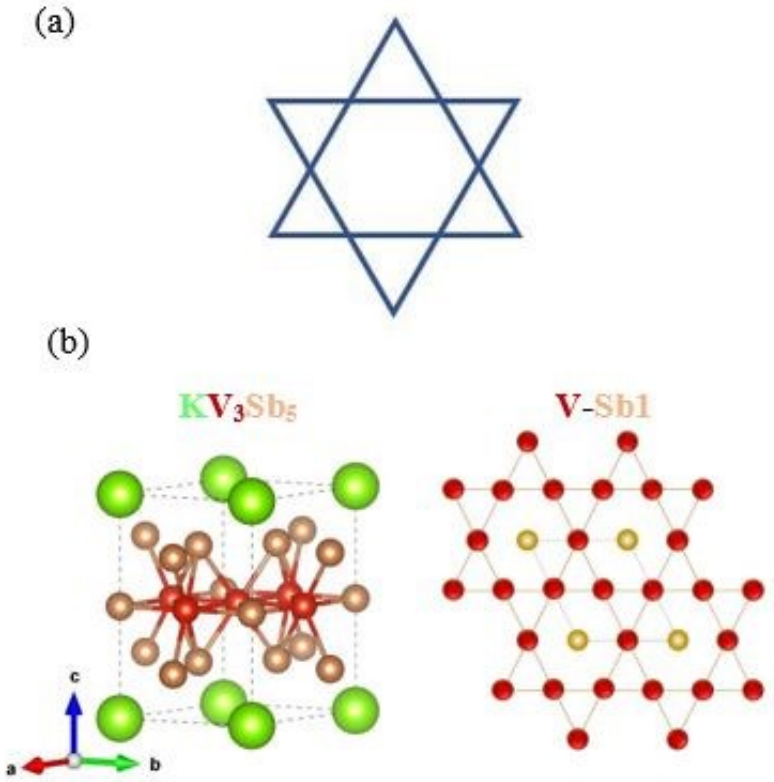

Figure 1: (a) Unit of kagomé lattice structure, and (b) KV_3Sb_5 Unit Cell and Vanadium kagomé net showing Sb1 atoms centered on hexagons

The intensive study in pursuit of confirmation of a quantum spin liquid state is especially true for kagomé materials of the insulating variety. However, several metallic kagomé materials have also been discovered. One such material is KV_3Sb_5. This compound, along with RbV_3Sb_5 and CsV_3Sb_5, are members of a recently discovered family of kagomé metals.[4] The previous work showed KV_3Sb_5 exhibited a kagomé sublattice of V. The material has two Sb sublattices, a simple hexagonal net at the same Z position as the V (formed by Sb1), and a graphene-like sublattice (formed by Sb2) above and below the kagomé net. Potassium is intercalated between the slabs of V-Sb. The previous work also calculated the band structure of the material. Calculations showed several Dirac points near E_F, highlighting potassium deintercalation as a potential means of tuning E_F.

Previous *uncontrolled* deintercalation treatments of this material have included etching with hot HNO_3, as well as treatment with water.[4] Effective *controlled* deintercalation of alkali metals with I_2 has been well established in related layered materials.[5-7] In this work, we report on the deintercalation of potassium from KV_3Sb_5 via $[I_2 + I^-]$ in acetonitrile (ACN). Examination of the change in c/a ratios with varying degrees of initial electrochemical potential of solution indicates a gradation of the extent of deintercalation. However, a degree of decomposition of the material was also observed, and limits the precision to which potassium content can be tuned. There was also a noticeable trend in the behavior of the magnetic susceptibility at $T \approx 2K$ with increasing initial electrochemical potential of solution.

Methods

KV_3Sb_5 powder was initially synthesized by Ortiz et al by ball milling all elemental reagents together.[4] In this work, a multi-step solid state reaction process was used. V (foil, 99.5%) and Sb (shot, 99.999%) were pressed into a 6mm pellet to 5000 psi and held for 5 min. Approximately 10% excess of Sb was added above the V_3Sb_5 stoichiometry to account for loss due to the relatively high vapor pressure of Sb. Pressed pellets were heated to 1100°C for 16 hours in evacuated quartz ampoules.[8] Products of this reaction, in addition to K (ingot, 99.8%), were then hand-pressed into a pellet in a glovebox. Approximately 10% excess K was added above the KV_3Sb_5 stoichiometry, using initial V content as the reference. Pellets were heated to 400°C for 1 hr in evacuated quartz ampoules to react all elemental K. Products of this reaction were removed from the ampoule, ground, then pressed into 6mm pellets to 5000 psi for 5 min. These pellets were annealed at 600°C for 48 hours in evacuated quartz ampoules.

Phase purity was checked with Powder X-ray diffraction (PXRD) data collected at room temperature. This was done using Bruker D8 Focus diffractometer with a LynxEye detector using Cu Kα radiation. Rietveld refinements on the PXRD data were done through TOPAS 4.2 (Bruker).

Three solutions of $[I_2 + I^-]$ in ACN were prepared with differing amounts of $I_2 + I^-$. Solution A contained I_2 to match half the stoichiometry of K in KV_3Sb_5 (+5% excess) dissolved in 17 ml of ACN in a small vial. Sample B contained both I_2 and KI in a ratio of 2:1, and contained I_2 in an amount to match the stoichiometry of K in KV_3Sb_5 (+5% excess) dissolved in 17 ml of ACN in a small vial. Sample C contained both I_2 and KI in a ratio of 2:1, and contained I_2 in an amount to match half the stoichiometry of K in KV_3Sb_5 (+5% excess) dissolved in 17 ml of ACN in a small vial. Ground KV_3Sb_5 powder was added to each of these solutions, sealed,

and left to stir for 4 days at room temperature. Samples were then filtered using a Buchner funnel, rinsed with ACN, and dried.

Manual subtraction of XRD data and Peak fitting were done in Fityk 1.3.1.

Magnetic Susceptibility data was collected using the Quantum Design Physical Properties Measurement System (PPMS) using the AC transport option with an applied DC field of $\mu_0 H = 10$ Oe, and an AC drive field of 3 Oe at a frequency of 1000 Hz.

Results

A Structure Confirmation

Prior to deintercalation, phase-pure KV_3Sb_5 had to be synthesized. Due to a combination of contamination and safety concerns with respect to ball milling (ball milling often introduces 3-5% of the ball material into mixtures, and clean potassium can be very reactive when spread out into a thin film), it was decided to pursue a different synthesis route than used in previous work.[4] Room temperature PXRD data of the product of multi-step solid state synthesis route was collected. A Rietveld refinement of the previously reported P6/mmm spacegroup and parameters to the PXRD data (Figure 2) confirmed phase purity. The non-uniform background is due to a

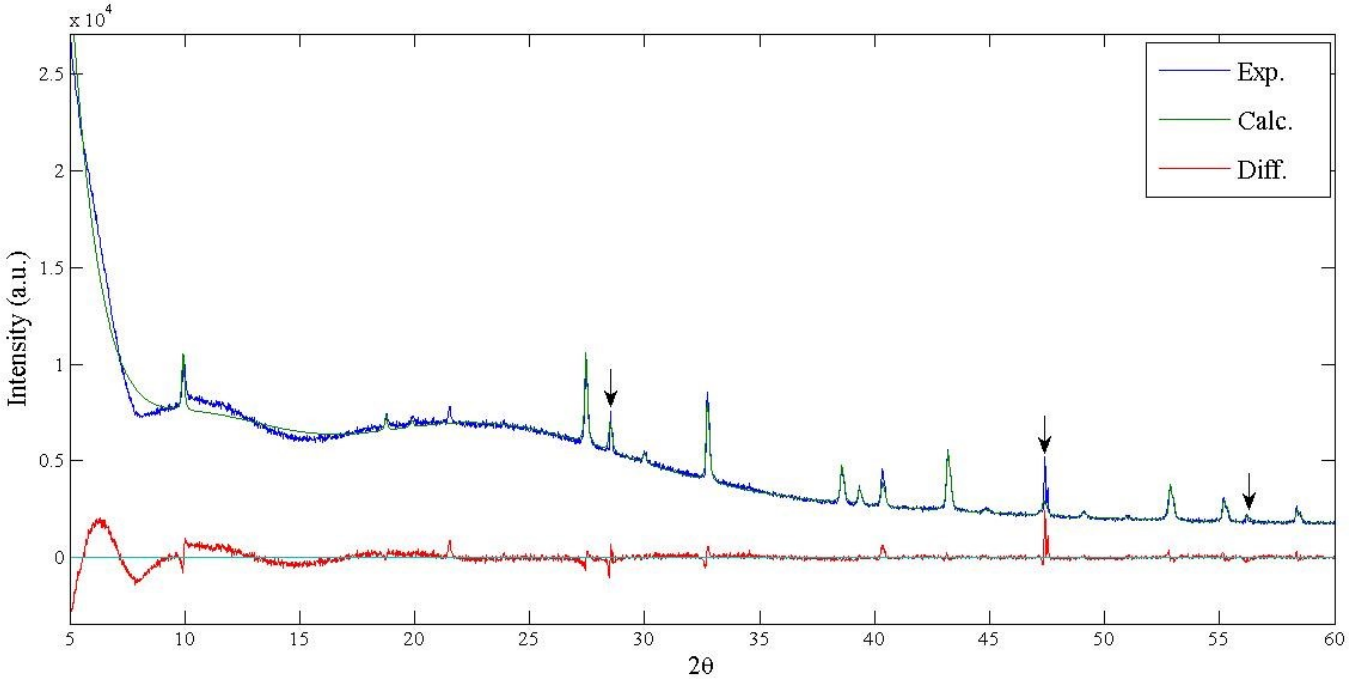

Figure 2: Rietveld Refinement confirming phase purity of synthesis method with arrows indicating peaks associated with the added Si standard

combination of the instrument configuration and sample prep necessitated due to the water sensitivity of the material.

A reference standard of crystalline Si was added to the KV_3Sb_5 powder sample for the PXRD measurements to ensure accurate lattice parameter data. The Crystal data and calculated Lattice parameters resulting from this refinement are presented in Table 1. As there are only three free parameters (the Sb2 z coordinate and a and c lattice parameters), a reasonable refinement was obtainable. The atomic displacement parameters were fixed at Uiso = 0.006.

Table 1: Crystal Data and Lattice parameters of first successful powder

Atomic Coordinates			
Site	X	Y	Z
K1	0	0	0
V1	1/2	1/2	1/2
Sb1	0	0	1/2
Sb2	2/3	1/3	0.7595(15)
Lattice Parameters			
a (Å)		5.47536(30)	
c (Å)		8.94577(89)	

After confirmation of the synthesis method, more samples were made. Figure 3 shows the Rietveld refinements of the samples that were subsequently used for deintercalation experiments. The top refinement is of KV_3Sb_5 Sample 1, the parent compound of deintercalation Sample A. The bottom refinement is of KV_3Sb_5 sample 2, the parent compound of deintercalation Samples

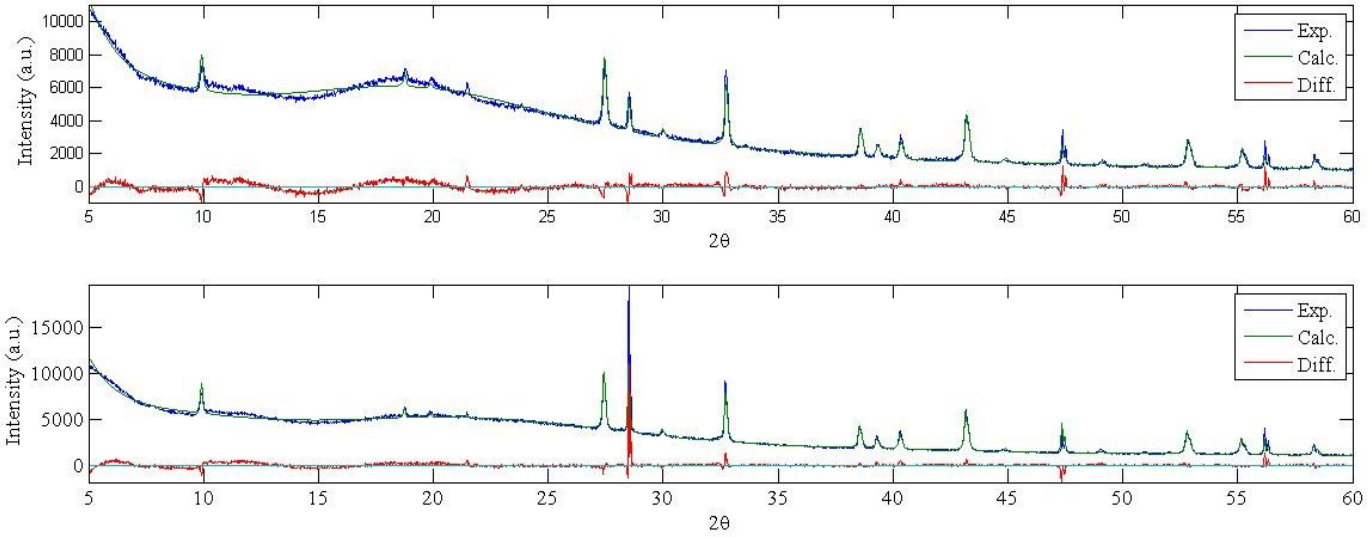

Figure 3: Rietveld refinements of the two samples used for deintercalation, Sample 1 (top) and Sample 2 (bottom). The large discrepancy between the data and model at 2θ≈28 is a result of excess reference Si powder added to the sample.

B and C. The crystal data and lattice parameters for these two KV_3Sb_5 samples are presented in Table 2.

Table 2: Crystal Data and Lattice parameters for the 2 KV_3Sb_5 samples used for deintercalation

Atomic Coordinates - Sample 1				**Atomic Coordinates - Sample 2**			
Site	X	Y	Z	Site	X	Y	Z
K1	0	0	0	K1	0	0	0
V1	1/2	1/2	1/2	V1	1/2	1/2	1/2
Sb1	0	0	1/2	Sb1	0	0	1/2
Sb2	2/3	1/3	0.76363(86)	Sb2	2/3	1/3	0.7595(15)
Lattice Parameters				**Lattice Parameters**			
a (Å)		5.47597(23)		a (Å)		5.47989(19)	
c (Å)		8.94704(68)		c (Å)		8.95485(58)	
c/a		1.63387		c/a		1.63413	

B Deintercalation

Using thermodynamic data obtained from potentiometric measurements of [I_2 + I^-] in ACN, the the initial electrochemical potentials of the solutions used for deintercalation were calculated using equation 1.[9]

$$E = (\varepsilon_{02}^{'} - \varepsilon_{01}^{'}) + \frac{RT}{2F} \ln \left[\frac{\left(m_{I_2,2} - m_{I^-}^0\right)^3 \left(m_{I^-}^0 - m_{I_2,1}^0\right)^3}{(m_{I^-}^0)^2 (m_{I_2,1}^0)} \right] + (\varepsilon_{j2} - \varepsilon_{j1}) \qquad (1)$$

Failamani et al showed that calculations using the approximations utilized in this relationship are

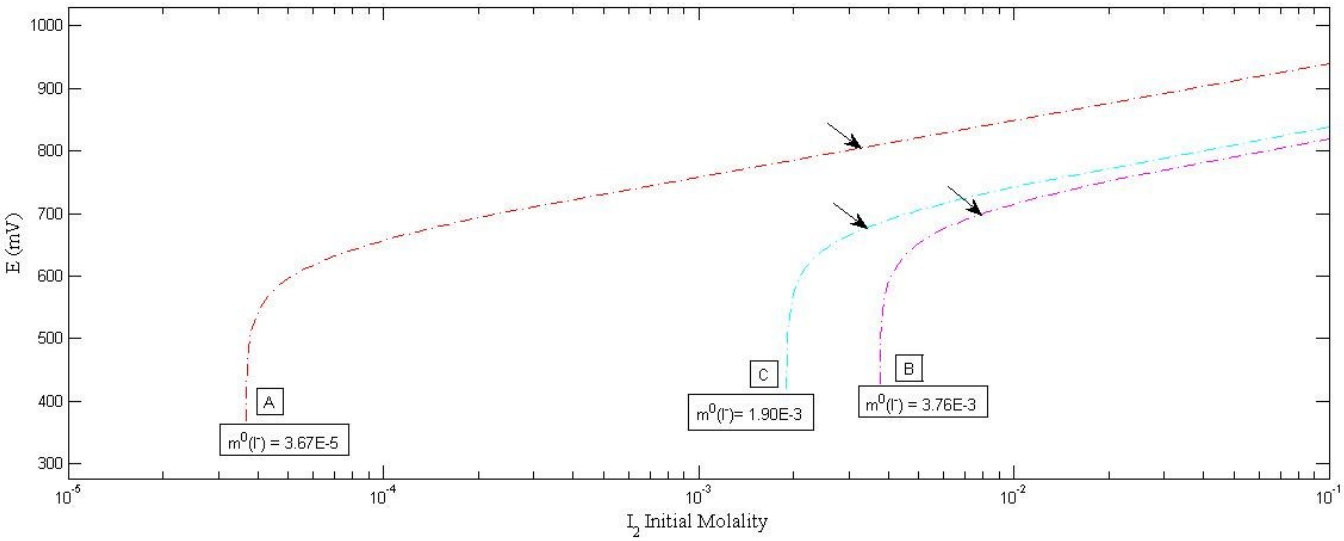

Figure 4: Electrochemical potentials for fixed initial I- molality at varying I_2 initial molalities calculated from equation 1. The three curves represent the 3 initial I^- molalities used for deintercalation. Arrows show the approximate point on each curve that represents the initial I_2 concentration and electrochemical potential.

in good agreement with the measured potentials, particularly in the region of the curves studied in this work.[9]

Figure 5 shows the Rietveld refinements of the 3 deintercalated samples. Table 3 lists the lattice parameters of these three samples.

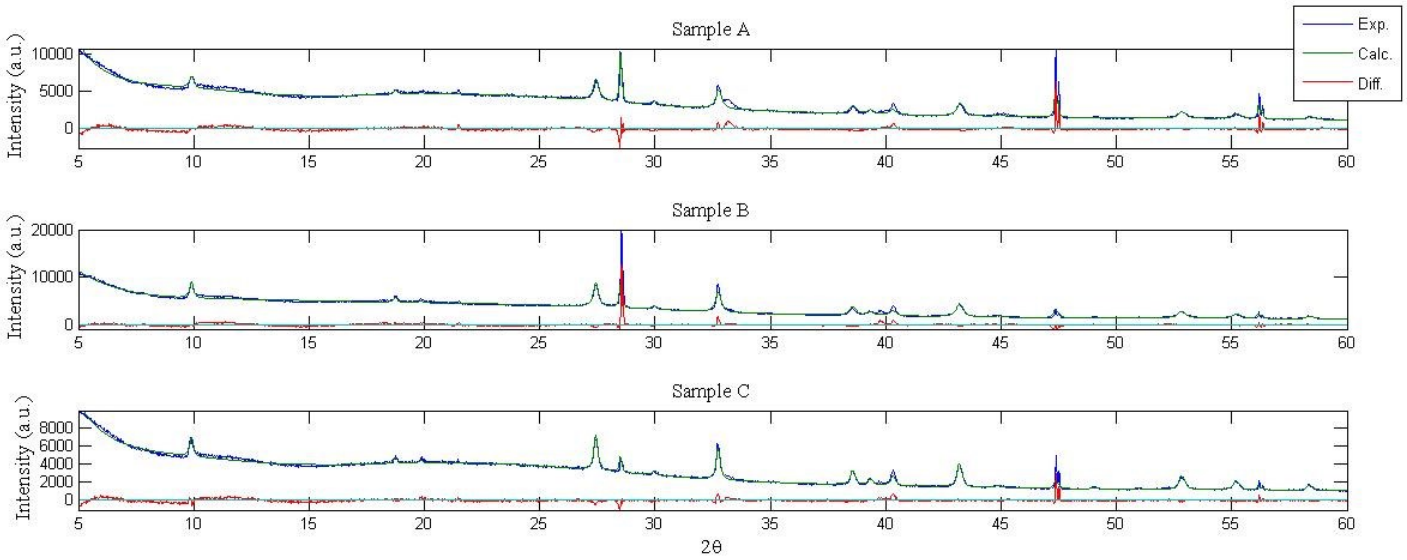

Figure 5: Rietveld Refinement of Samples A, B, and C after deintercalation, filtering, and drying

Table 3: Lattice parameters of deintercalated samples

Lattice Parameters			
	Sample A	Sample B	Sample C
a (Å)	5.47317(64)	5.47656(48)	5.47804(25)
c (Å)	8.9547(20)	8.9562(14)	8.95623(76)
c/a	1.63611	1.63537	1.63493
Δ c/a	.0022335	.0012401	.000804

The ratio of lattice parameters c/a was used as a proxy for potassium occupancy. The change in c/a was used as opposed to c/a to help mitigate the effects of using two different parent samples of KV_3Sb_5. Figure 6 shows the relationship between Δc/a and the starting electrochemical solution of the $[I_2 + I^-]$ in ACN.

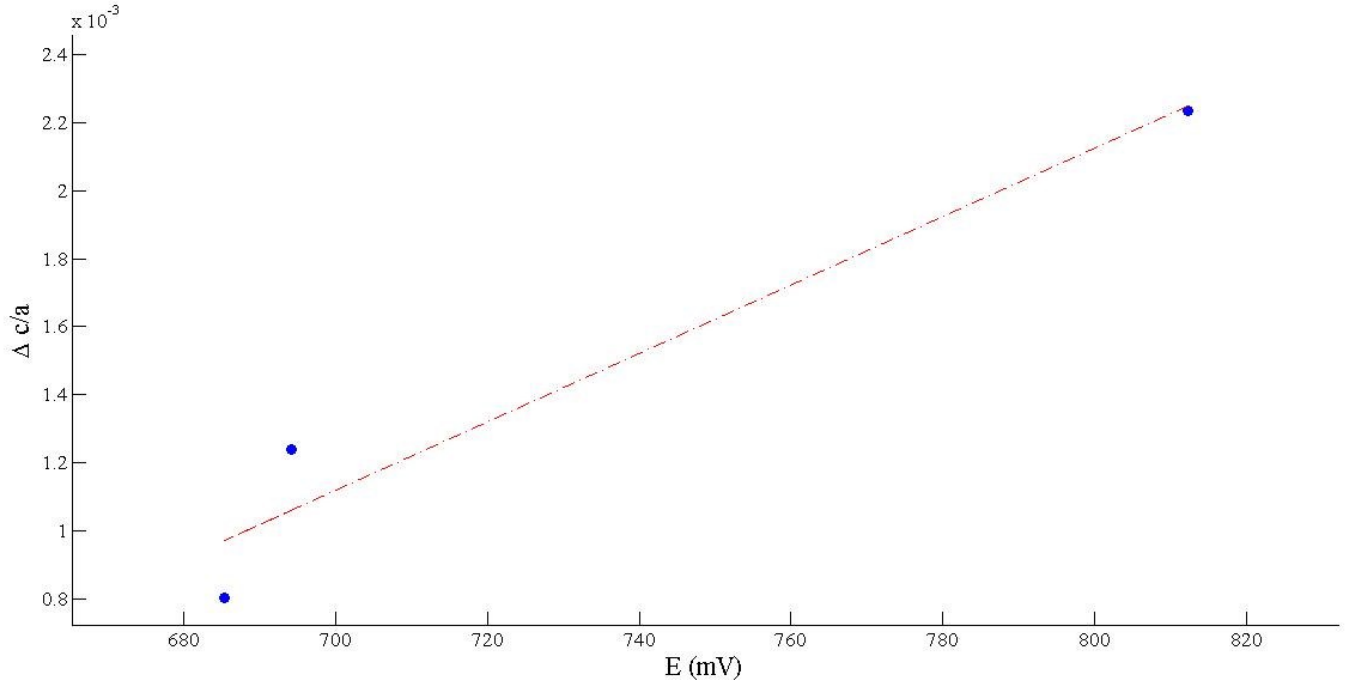

Figure 6: Δ c/a vs electrochemical potential

C Decomposition

It was noticed that the peak at 2θ≈32 displayed the budding of a secondary peak, indicating a degree of decomposition of material. This secondary peak formation was most apparent in sample A (Figure 7).

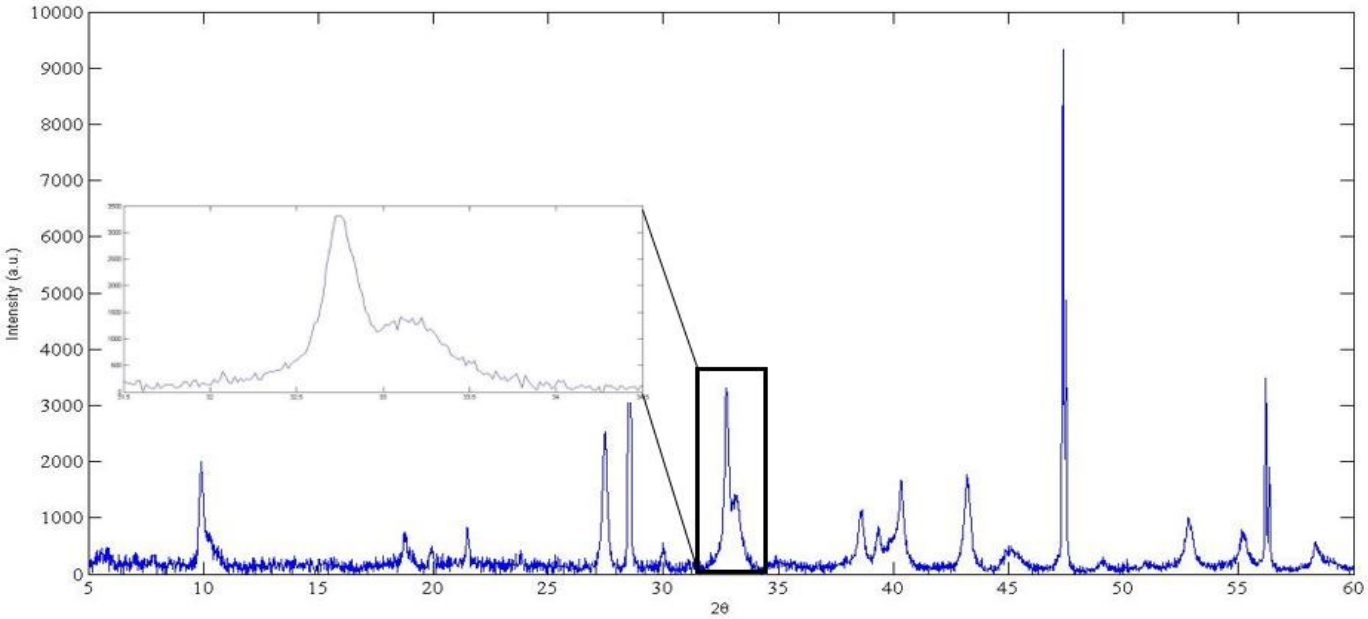

Figure 7: Raw XRD data from sample A with manually subtracted background and inset showing the peaks to be analyzed for decomposition

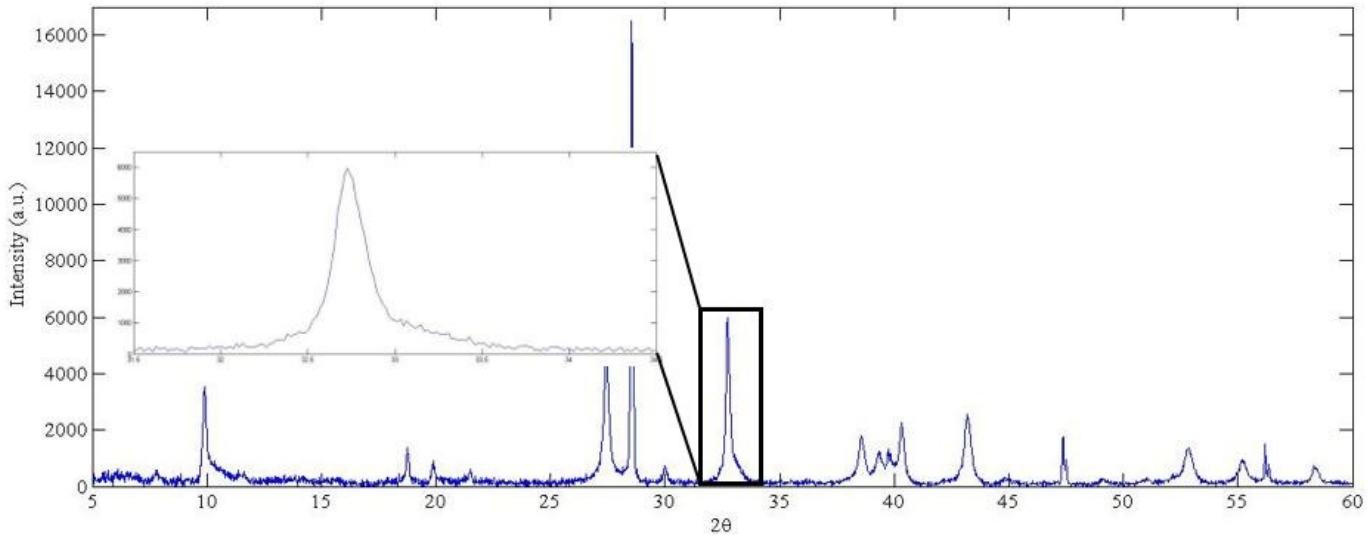

Figure 8: Raw XRD data from sample B with manually subtracted background and inset showing the peaks to be analyzed for decomposition

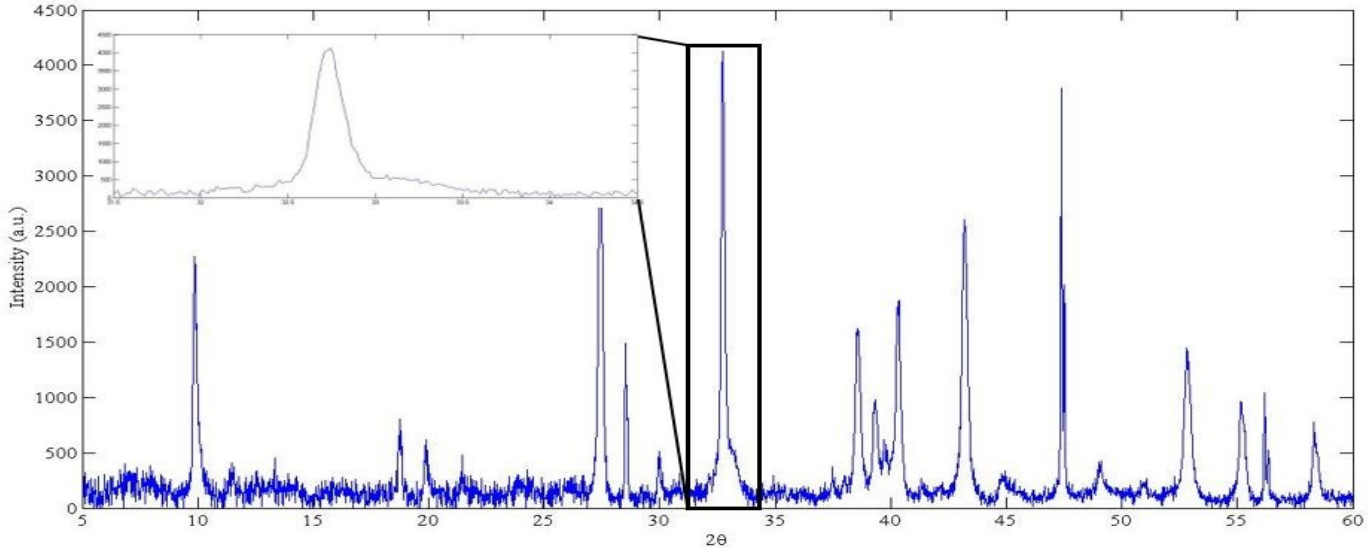

Figure 9: Raw XRD data from sample C with manually subtracted background and inset showing the peaks to be analyzed for decomposition

The two curves were fit with split pseudo-Voight curves Figure 10. As the secondary peak

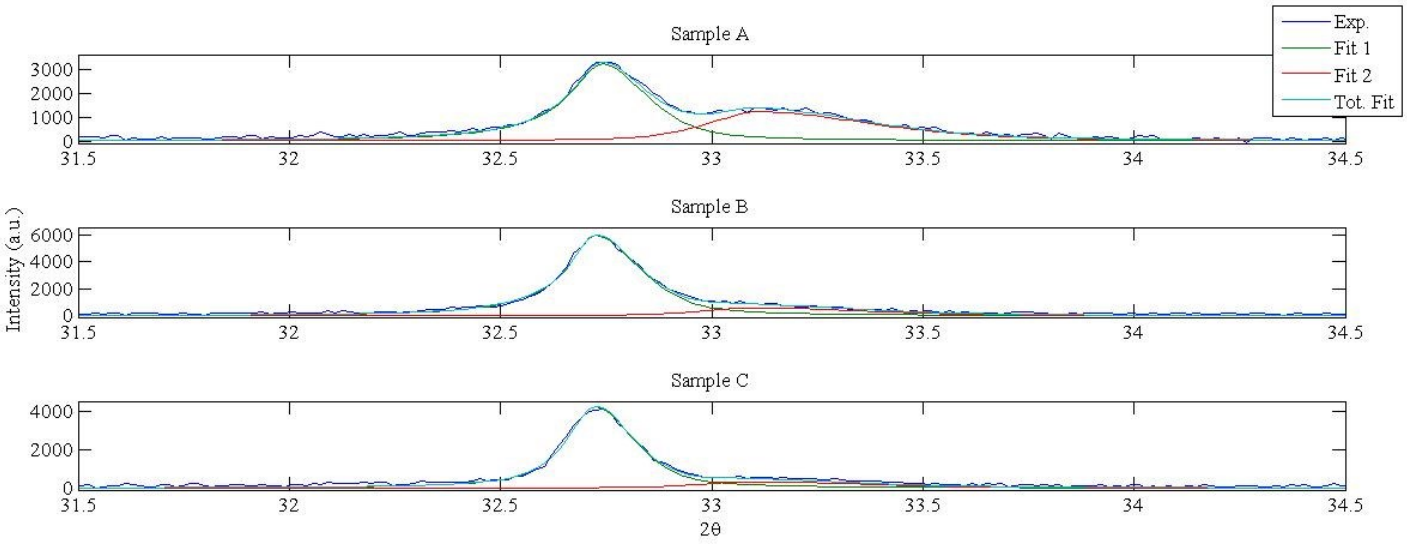

Figure 10: Split Pseudo-Voight curves fit to the decomposing peak for each sample

formation was most promionent for sample A, the secondary peak centers for sample B and C were fixed at the same distance from the primary peak as in sample A. Peak fit heights are presented in Table 4.

Table 4: Heights of the fit peaks as well as the ratio of peak heights

	Sample A	Sample B	Sample C
Primary Peak Height	3246	4245	5970
Secondary Peak Height	1225	339	598
Decomposition Ratio	0.377	0.080	0.100

The ratio of secondary peak height to primary peak height was used as a quantification metric for degree of decomposition. When these ratios were plotted vs electrochemical potentials of deintercalation solutions, the relationship was surprisingly strong (Figure 11).

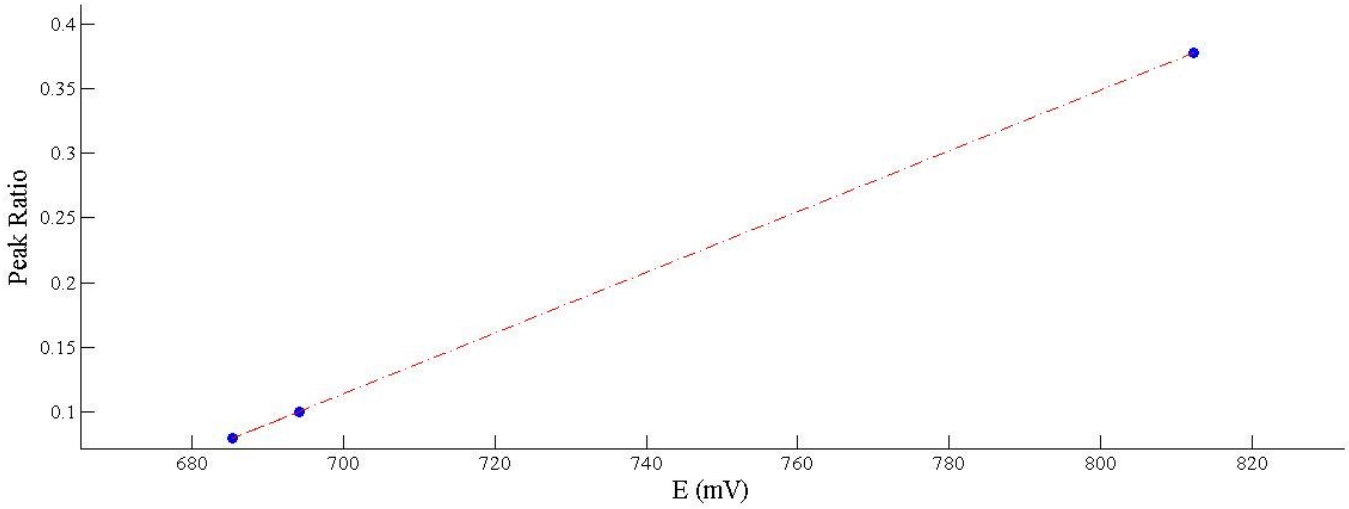

Figure 11: Decomposition vs Electrochemical potential of deintercalation solution

D AC Susceptibility

AC magnetic susceptibility measurements were taken for deintercalation samples A, B and C (Figure 12). The magnitude of the measurements for samples A and B were about an

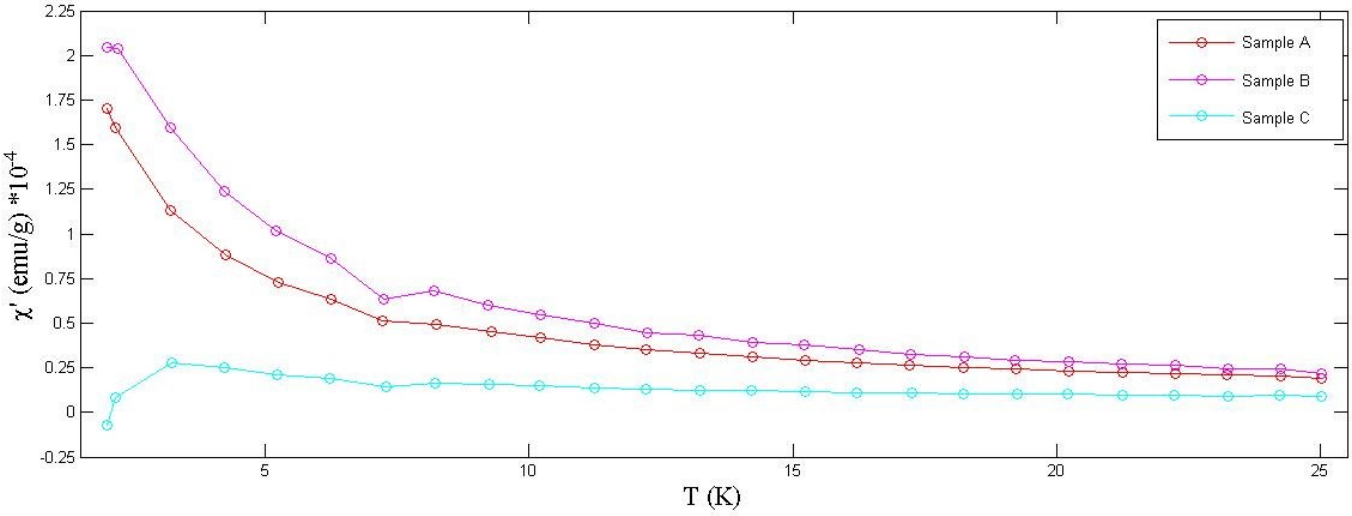

Figure 12: Magnetic Susceptibility data, showing a change in behavior around 2K with varying electrochemical potentials of deintercalation solution

order of magnitude greater than that of sample C, with sample B being slightly greater than Sample A. The curves indicate paramagnetic behavior in all of the samples above ≈3K.

However, below this temperature, behavior deviates. Sample A continues the behavior seen at greater temperatures. Sample B displays a slight change just above 2K, and sample C shows a significant change around the same temperature, with susceptibility going negative, possibly indicating the beginnings of a superconducting transition. Previously, single crystal measurements of KV_3Sb_5 have shown the material to be superconducting with a $T_C \approx 0.93K$.[10] As sample C saw the least degree of deintercalation, superconducting behavior of the parent compound may still be observable. The greater degrees of deintercalation of samples A and B may have driven a more significant shift away from superconducting behavior at low temperatures. The differing susceptibility behavior may also be a result of the introduction of ferromagnetic influence of the decomposition products. However, this seems less likely, as sample A, with the greatest decomposition, shows behavior less indicative of this than sample B.

Discussion

Structural analysis confirmed that this multi-step method of KV_3Sb_5 synthesis was suitable. For the Rietveld refinements of PXRD data, the material's three structural degrees of freedom (a, c, and Sb2 position) were allowed to vary. Potassium occupancy was also allowed to vary; however, it was decided to use c/a ratio to glean K occupancy information, as crystallite

size was not fully controlled for and has a large effect on occupancy calculations via Rietveld refinement.

For deintercalation sample A, only I_2 was added to the ACN. However, in order to calculate the electrochemical potential of this solution, the initial concentration of I^- was approximated. It was assumed that 1 mol percent of the added I_2 would be reduced to I^-. Due to the logarithmic dependence of the electrochemical potential on the initial molalities even an order of magnitude above/below this estimate does not have a large effect.

Future studies would benefit from more refined control of I^- concentrations for the "higher" solution potentials. Also, a larger set of data points along the range of potentials would improve the analysis. Ideally the same sample would have been used for all of the deintercalation conditions. However, significant sample loss on filtering prevented this. Future studies would benefit from use of the same parent sample for subsequent deintercalation experiments.

Each deintercalation did show a change in potassium occupancy, showing a positive, yet non-linear, relationship to electrochemical driving force. However, this change in occupancy was accompanied by a degree of decomposition that did increase linearly with electrochemical driving force. While a more robust method of identifying decomposition extent and products is warranted, attempts to mitigate this decomposition should be considered for future work.

The deintercalation reaction is not diffusion-limited, so changing the duration is unlikely to have a significant effect. However, the effects of temperature may be a good direction of study for future work.

Conclusion

The successful controlled deintercalation of potassium from the kagomé metal KV_3Sb_5 via $[I_2 + I^-]$ in ACN is reported. By examining the change in lattice parameter ratios (c/a), it was seen that greater degrees of deintercalation were achieved with greater initial electrochemical potential of deintercalation solution. While this is encouraging for the tunability of the kagomé metal, a greater degree of deintercalation was accompanied by a greater degree of decomposition of the parent material. Additionally, significant differences in magnetic susceptibility measurements at very low temperatures (< 3K) were observed between samples, indicating an apparent shift away from superconductivity with greater degree of deintercalation. Magnetic measurements at temperatures below 2K for gradated deintercalations of KV_3Sb_5 are a possible area of future work.

References

(1) Balents, L. Spin Liquids in Frustrated Magnets. *Nature* **2010**, 464, 199−208

(2) Broholm, C.; Cava, R. J.; Kivelson, S. A.; Nocera, D. G.; Norman, M. R.; Senthil, T. Quantum spin liquids. *Science* **2020**, 367, eaay0668

(3) Chamorro, J. R.; McQueen, T. M.; Tran, T. T. Chemistry of Quantum Spin Liquids, *Chem. Rev.* **2021**, 121, 5, 2898-2934

(4) Ortiz, B. R.; Gomes, L. C.; Morey, J. R.; Winiarski, M.; Bordelon, M.; Mangum, J. S.; Oswald, I. W. H.; Rodriguez-Rivera, J. A.; Neilson, J. R.; Wilson, S. D.; Ertekin, E.; McQueen, T. M.; Toberer, E. S. New Kagomé Prototype Materials: Discovery of KV_3Sb_5, RbV_3Sb_5, and CsV_3Sb_5. *Phys. Rev. Materials* **2019**, 3, 094407

(5) Murphy, D.W.; Cros, C.; Di Salvo, F. J.; Waszczak, J. Preparation and Properties of LixVS2 ($0 \leq x \leq 1$), *Inorg. Chem.* **1977**, 16, 3027

(6) Schleich, D.M. Chimie douce: Low temperature techniques for synthesizing useful compounds, *Solid State Ionics* **1994**, 70–71, 1, 407-411

(7) Neilson, J. R.; McQueen, T. M. Bonding, Ion Mobility and Rate-Limiting Steps in Deintercalation Reactions with ThCr2Si2-type KNi2Se2, *J. Am. Chem. Soc.* **2012**, 134, 18, 7750-7757

(8) Failamani, F.; Broz, P.; MacCiò, D.; Puchegger, S.; Müller, H.; Salamakha, L.; Michor, H.; Grytsiv, A.; Saccone, A.; Bauer, E.; Giester, G.; Rogl, P. Constitution of the systems {V,Nb,Ta}-Sb and physical properties of di-antimonides $\{V,Nb,Ta\}Sb_2$, *Intermetallics* **2015**, 65, 94-110

(9) Baucke, F.G.K.; Bertram, R.; Cruse, K. The iodide-iodine system in acetonitrile: Evaluation of standard thermodynamic data on the association $I^- + I_2 \rightarrow I_3^-$ from potentiometric measurements at 25 and 50°C, Journal of Electroanalytical Chemistry and Interfacial *Electrochemistry* **1971**, 32, 2, 247-256

(10) Ortiz, B.; Sarte, P.R.; Kenney, E.M; Graf, M.J.; Teicher, S.M.L.; Seshadri, R.; Wilson, S.D. Superconductivity in the Z_2 kagomé metal KV_3Sb_5, *Phys. Rev. Materials* **2021**, 5, 3